ARL-TR-10186 • Sep 2025

Influence of Fatigue Damage on the Response of α-Fe to 1D Shock and Spall Loading

by Scott A. Turnage and Joseph Indeck

NOTICES

Disclaimers

ARL-TR-10186 ● SEP 2025

Influence of Fatigue Damage on the Response of α-Fe to 1D Shock and Spall Loading

Scott A. Turnage
DEVCOM Army Research Laboratory

Joseph Indeck
Boeing

REPORT DOCUMENTATION PAGE

1. REPORT DATE	2. REPORT TYPE	3. DATES COVERED START DATE	END DATE
September 2025	Technical Report	10/01/2019	4/30/2024

4. TITLE AND SUBTITLE
Influence of Fatigue Damage on the Response of α-Fe to 1D Shock and Spall Loading

5a. CONTRACT NUMBER	5b. GRANT NUMBER	5c. PROGRAM ELEMENT NUMBER
5d. PROJECT NUMBER	**5e. TASK NUMBER**	**5f. WORK UNIT NUMBER**

6. AUTHOR(S)
Scott A. Turnage and Joseph Indeck

7. PERFORMING ORGANIZATION NAME(S) AND ADDRESS(ES)	8. PERFORMING ORGANIZATION REPORT NUMBER
DEVCOM Army Research Laboratory ATTN: FCDD-RLA-TA Aberdeen Proving Ground, MD 21005	ARL-TR-10186

9. SPONSORING/MONITORING AGENCY NAME(S) AND ADDRESS(ES)	10. SPONSOR/MONITOR'S ACRONYM(S)	11. SPONSOR/MONITOR'S REPORT NUMBER(S)

12. DISTRIBUTION/AVAILABILITY STATEMENT
DISTRIBUTION STATEMENT A. Approved for public release: distribution unlimited.

13. SUPPLEMENTARY NOTES
ORCID: Scott A. Turnage, 0000-0001-9375-903X

14. ABSTRACT
The dynamic strengths of certain materials such as alpha (α)-iron (Fe) have been well studied, but while the damage imparted by shock and spall loading in pristine α-Fe is well known, hardly any effort has probed the influence of existing damage on the dynamic mechanical performance of the material. Here, α-Fe is subjected to varying degrees of fatigue loading resulting in differing levels of fatigue damage. Materials are then loaded under shock and spall with compressive shock stresses ranging from 6 to 16 GPa. The influence of voids formed by fatigue damage are discussed in terms of the influence on the Hugoniot elastic limit (HEL), phase transformation stress, and spall stress. Fatigue damage is shown to reduce the HEL but exhibits little influence on the phase transformation stress. Fatigue damage noticeably affects the spall strength by influencing the critical peak shock stress at which spall strength transitions from decreasing with increasing peak shock stress to increasing with increasing peak shock stress.

15. SUBJECT TERMS
dynamic impact, alpha-Fe, α-Fe, fatigue, spall, phase transformation, Terminal Effects

16. SECURITY CLASSIFICATION OF: a. REPORT	b. ABSTRACT	C. THIS PAGE	17. LIMITATION OF ABSTRACT	18. NUMBER OF PAGES
UNCLASSIFIED	UNCLASSIFIED	UNCLASSIFIED	UU	23

19a. NAME OF RESPONSIBLE PERSON	19b. PHONE NUMBER *(Include area code)*
Scott A. Turnage	(520) 691-5075

STANDARD FORM 298 (REV. 5/2020)
Prescribed by ANSI Std. Z39.18

Contents

List of Figures

List of Tables

Acknowledgments

We gratefully acknowledge the efforts of Dave Ayers, Jermaine Bradley, Jason Garvey, and Eric Wilson (ARL) in conducting the gas gun experiments. We are also grateful for many helpful discussions with Drs. Cyril Williams, Debjoy Mallick, and Jeffrey Lloyd (ARL), and Dr. Kavan Hazeli (University of Arizona).

1. Introduction

Damage resulting from continuous cycling of elastic loads can result in significant changes in a material's mechanical performance. For example, Lopez et al.[1] studied the effects of surface defects, including surface roughness and heat affected zones generated by machining processes in Ti-6Al-4V, on the reduction of mechanical properties resulting from fatigue loading. They found that, while fatigue loading imparts no noticeable change on the mechanical properties of the Ti-6Al-4V bulk material, cracks formed during fatigue loading in the surface layer that had been affected by the machining process. These cracks result in the degradation of strain to failure. Kawata et al.[2] measured the quasi-static and dynamic mechanical response of three aluminum alloys—2219-T87, 7075-T7351, and 6061-T6—following fatigue damage generation. They found that none of the probed alloys exhibited any change under quasi-static tension, but aluminum alloys 2219-T87 and 7075-T7351 exhibited a loss of tensile strength under high-rate tension while 6061-T6 showed no influence of fatigue damage on mechanical response at any strain rate. Strain hardening and local stress concentrations were the proposed deformation mechanisms responsible for the changes in mechanical response.

While Ti-6Al-4V with a cleaned surface and 6061-T6 show little influence from fatigue, other materials show significant changes in microstructure owing to fatigue damage. Paul et al.[3] probed the effect of low-cycle fatigue and ratcheting on the deformation of 304LN stainless steel and found that plastic strain from cyclic deformation resulted in hardening in fatigue-loading scenarios. This was demonstrated by the increase in tensile yield and ultimate strengths as well as a reduction in the cyclic strain of the observed hysteresis loop with increasing number of load cycles. When loaded under tension to failure, specimens with prior low-cycle fatigue loading exhibited a few large dimples on the fracture surface while specimens with prior ratcheting deformation exhibited a significantly increased number of small dimples. As would be anticipated, this implies that ratcheting deformation results in more extensive nucleation of damage sites than low-cycle fatigue.

Changes in microstructure generally result in changes in mechanical performance. Sanchez-Santana et al.[4] investigated the influence of fatigue damage on the quasi-static and dynamic response of 6061-T6 aluminum alloy and American Iron and Steel Institute (AISI) 4140T steel. They found that increased fatigue damage lowers the yield and ultimate strength of each material. However, ductility in 6061-T6 increased with additional fatigue damage irrespective of strain rate while ductility decreased in the strain-hardened AISI 4140T steel with additional fatigue damage at both quasi-static and high strain rates.

The differing results from Kawata et al.[2] and Sanchez-Santana et al.[4] likely result from the differing paths to achieve the fatigue damage in the 6061 material. Therefore, resolution of the effects of fatigue damage on the mechanical response requires an understanding of the fatigue damage imparted by fatigue loading. Duyi and Zhenlin[5] studied the microstructure and mechanical properties developed at varying levels of fatigue deformation in medium-carbon steel. Their findings reveal significant changes in mechanical response resulting from significant dislocation generation and accumulation. Static toughness—a parameter influenced by the ultimate stress, strain hardening, and area reduction—is most affected by the amount of fatigue damage.

While efforts continue to elucidate the effects of fatigue damage on material failure under uniaxial stress loading conditions, a paucity of research has been performed to understand fatigue damage effects on material shock and spall response where loading is limited to uniaxial strain conditions. Of particular interest are iron (Fe)-based materials common in applications where dynamic loading is plausible and in which effects of fatigue damage have been previously noted in lower strain-rate experiments.[4,5] Undamaged alpha (α)-Fe, which is particularly useful for a basic understanding of Fe-based materials, has been extensively studied under dynamic loading. For example, Barker and Hollenbach[6] investigated α-Fe at pressures from 10 to 40 GPa peak shock pressures with a focus on the phase transformation stress, finding the phase transformation from body-centered cubic (BCC) to hexagonal close-packed crystal structure occurs at approximately 13 GPa. Thomas et al.[7] investigated the dynamic compression response of α-Fe within the α phase to determine a shock Hugoniot, Hugoniot elastic limit (HEL), and spall strength in 8-mm-thick specimens. However, despite extensive research in α-Fe, the effects of preexisting damage on the mechanical performance of α-Fe under dynamic uniaxial strain are not well understood. Thus, they are the impetus of the experimental investigation detailed here.

Microscale plasticity results in localized damage formation during high-cycle elastic loading.[8] This plasticity creates localized accumulation of dislocation clusters which, as cyclic loading continues, can progress to nucleate and grow voids within the material (primarily at grain boundaries). The resultant damage then reduces a material's ability to withstand high static load and failure occurs at stresses below the failure point of the undamaged material. Indeck et al.[9] investigated α-Fe for the progression of damage with an increase in loading cycles. They found voids existed in the undamaged material and cyclic loading increased void size, occurring most notably above 73% of the number of cycles to failure. This work uses the same material under the same conditions as that described in Indeck et al.,[9] so the microstructures and internal defects should be analogous.

The response of materials to shock load is highly dependent on the microstructure of the material. In body-centered cubic (BCC) metals, annealed specimens exhibit higher HEL than in worked material.[10,11] For materials that undergo a pressure-induced phase transformation (e.g., Fe-based alloys), alloying can result in either increased or decreased phase transformation stress.[12] Also, the compressive strain rate during shock loading can influence the phase transformation stress, though to a lesser extent.[13] However, the effect of preexisting damage on the phase transformation is still uncertain.

Another important consideration of damage from shock loading is that of spall; i.e., the convergence of rarefaction fans from release of the shock wave at the free surfaces of the impactor and target, respectively. Spall strength is typically reduced as the size and density of the largest inhomogeneities (particle inclusions,[14] grain boundaries,[15] etc.) are increased with high-purity, single-crystal materials exhibiting the greatest spall strengths for a given material class.[15] Feasibly, preexisting damage could become a nucleation site for spall damage if no larger inhomogeneity exists. Furthermore, existing damage in the form of voids could influence the response to shock load because dynamic compression of voids results in recrystallization as a result of local high temperatures and significant damage states.[16] Despite the significant changes that preexisting damage can impart in the internal structure, few studies have investigated the effect of such damage on the spall response of materials. Surprisingly, investigations into the effect of preexisting damage on the response of materials to shock load in general are sparse. Lloyd et al.[17] found that shock loading a magnesium alloy with initially embedded twins results in damage accommodated by further twin nucleation and growth. However, a shock passing through the same magnesium alloy initially treated to remove twins prior to shock load does not retain any twins that may have formed during the shock loading, indicating possible detwinning as the deformation mechanism.

To further the work of addressing the effects of preexisting damage on the response of materials to dynamic uniaxial strain, specimens of α-Fe with varying levels of fatigue damage are investigated here under shock and spall loading at pressures below and above the phase transformation. Fatigue damage is applied under the same loading conditions but interrupted at differing percentages of the anticipated fatigue life to generate the differences in fatigue damage. HEL, phase transformation, and spall strengths are discussed with respect to changes resulting from fatigue damage.

2. Methods

Specimens of 99.8% pure Fe were prepared for fatigue loading following ASTM E466 guidelines.[18] For α-Fe, fully reversible cyclic loading was applied at 1 Hz to a peak stress of 285 MPa, corresponding to 70% of the yield stress. Fully reversible loading results in a zero mean stress and a stress ratio of R = –1. An initial specimen is loaded to failure under these conditions to determine the number of load cycles to failure (N_f) and subsequent specimens are loaded to a given number of load cycles (N) such that N/N_f equals 0.31, 0.62, 0.83, and 0.94, respectively. Greater detail of the fatigue loading in this work is found in Indeck et al.[9]

Plate impact experiments measure the response of the material to shock and spall loading. Details of the targets, impactors, impact velocities, and peak stress states are given in Table 1. 4340 steel impactors were propelled down the barrel of a light gas gun toward the target for nominal impact velocities of 300, 500, 700, and 900 m/s corresponding to peak shock stresses of approximately 6, 10, 13, and 16 GPa, respectively. Specimens were aligned such that planar impact was achieved within 5 mrad as verified by ionization pins. Specimen free-surface velocity was measured by a velocity interferometer system for any reflector (VISAR) below 13 GPa. However, later experiments performed well above the phase transformation stress were conducted using heterodyne-shifted photon Doppler velocimetry (PDV) rather than VISAR because the laboratory shifted the primary velocimetry measurement method from VISAR to PDV during this work's long time frame. Static elastic wave speeds were measured using ultrasonic techniques enabling an estimate of the shock velocity (U_s) based on the breakout times of the elastic (t_e) and inelastic (t_s) shock fronts following Equation 1

$$U_s = \frac{h}{h/c_l + (t_s - t_e)} \tag{1}$$

where h is the specimen thickness and c_l is the static longitudinal elastic wave speed.

Table 1. Parameters for each experiment.

Shot no.	Fatigue life (%)	h_t (mm)	h_i (mm)	v_0 (km/s)	σ (GPa)
y1953	0	4.422	2.976	0.340	6.7
y1954	0	4.360	2.916	0.509	9.6
y1955	0	4.436	2.968	0.661	13.1
b2408	0	4.487	3.013	0.884	16.4
y1947	31	4.416	2.964	0.317	6.1
y1948	31	4.422	2.964	0.507	9.9
y1951	31	4.376	2.972	0.677	13.3
b2409	31	4.436	3.008	0.887	15.8
y1961	62	4.230	2.974	0.317	6.1
y1962	62	4.406	2.968	0.505	9.3
y1956	62	4.544	2.966	0.668	13.1
b2410	62	4.427	3.008	0.893	15.6
y1946	83	4.196	2.968	0.329	6.1
y1949	83	4.334	2.964	0.495	9.8
y1950	83	4.500	2.962	0.669	13.8
b2413	83	4.366	3.020	0.887	15.0
y1964	94	3.518	2.984	0.312	6.0
y1965	94	3.454	2.978	0.507	9.7
y2005	94	3.558	2.960	0.683	13.1
b2414	94	2.832	3.026	0.896	16.5

Note: h_t = target thickness, h_i = impactor thickness, v_0 = impact velocity, σ = resulting peak shock stress.

Impact at the velocities investigated in this work results in a superposition of multiple waves corresponding to different stress jumps defined by the HEL, phase transformation stress (for the highest velocity experiments that surpass the transformation stress threshold), and the peak shock state that corresponds to the Hugoniot stress. As such, appropriate analysis requires employment of the generalized form of the jump Hugoniot equations applied for each stress wave. This process is well summarized in other works,[19,20] so it is not further discussed here.

Since fatigue experiments were performed according to ASTM E466[18] with a gauge section diameter of nominally 10 mm, keeping a 1:5 thickness-to-diameter ratio typical for plate impact experiments requires a thickness no greater than 2 mm. Furthermore, for spall experiments, an impedance matched impactor must have a smaller thickness than the target. Small targets and impactors complicate maintaining planarity and alignment. A ring of unfatigued α-Fe was press-fit around the fatigued specimen to ensure high-fidelity measurements without performing excessive fatigue experiments (Figure 1), thus enabling probing of the shock response of thicker materials. The effectiveness of this setup was investigated by comparing the results for as-received α-Fe with the same material using a standard geometry specimen nominally 6-mm-thick and 30 mm in diameter. The results will be discussed in the following section.

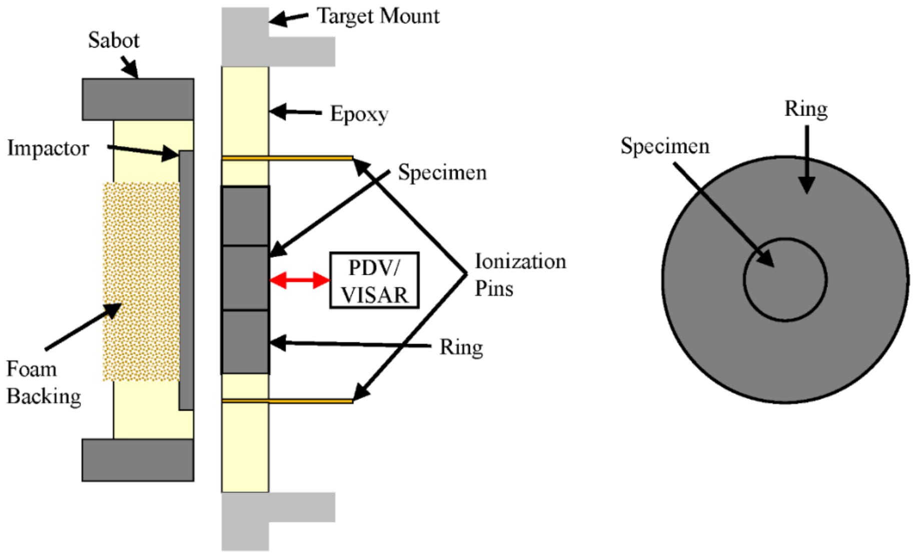

Figure 1. (Left) schematic of the normal plate impact experiment. Impact tilt remains <5 mrad as measured by ionization pins. VISAR or PDV measures the free-surface velocity. (Right) schematic of the 10-mm-diameter specimen placed within an impedance-matched 30-mm-diameter ring. The thickness of both specimen and ring is 4 mm.

3. Results and Discussion

As shown in Figure 2a, the ring does not fully prevent release from interfering with the velocimetry results. Particularly at low impact velocity (V_0), the stable state of the small-diameter specimen with the ring does not attain the peak free-surface velocity of the standard specimen until just prior to release. However, this maximum free-surface velocity correlates reasonably well with the stable state measured from the standard dimension specimen at low V_0. Therefore, though the results at low V_0 must be discussed with a degree of uncertainty, spall measurements will still be reported for the purpose of qualitative comparison of trends in spall behavior with increasing peak shock stress. At higher impact velocities, the edge release is negligible to nonexistent, exhibiting only a minor perturbation in the stable state that is inconsequential to the analyses discussed in this work.

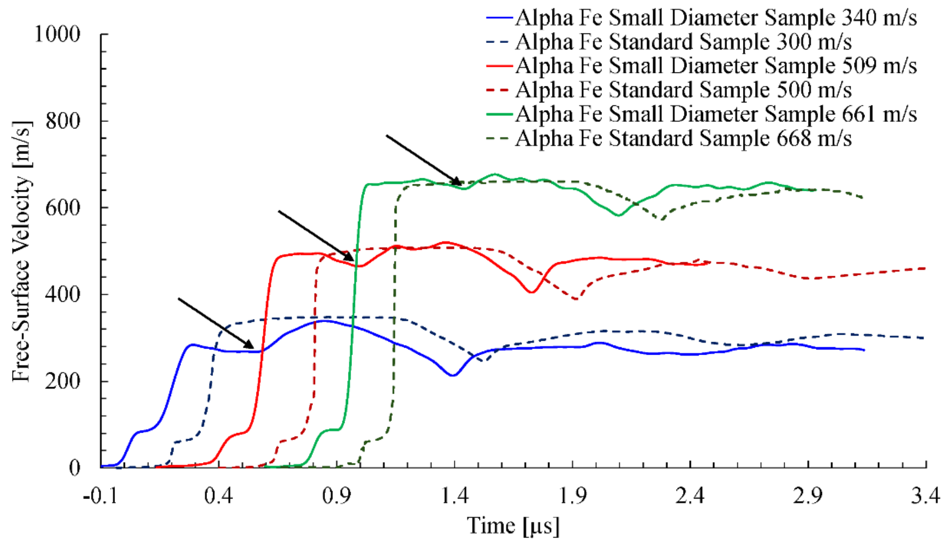

Figure 2. Comparison of experimental configurations on nonfatigued material. The timing of the curves is offset for clarity. Dashed lines represent results from a standard 30-mm-diameter × 6-mm-thick specimen. Solid lines represent results from a small-diameter specimen. Black arrows indicate perturbations resulting from release waves from the specimen press-fit ring interface.

Velocity–time profiles for each experiment in Figure 3 show a clear two-wave structure for specimens loaded below the phase transformation stress, denoting elastic and subsequent plastic waves. For the highest impact velocities, a three-wave structure is apparent (as reported numerous times in literature[6,10,13,19,20]) where the second wave increases the pressure in the material from the elastic state to the phase transformation stress, followed by the third wave that increases the stress in the material to the final Hugoniot state. A spall pulse is also clearly observed for each specimen. Particularly for the low-V_0 specimens, a dip is seen in the velocity once the plastic wave reaches the free surface, as previously discussed. For most cases, this dip is followed by a rise to the velocity corresponding to the peak stress state. This dip is believed to result from a weak edge release wave coming from the interface between the small-diameter specimen and the specimen holding ring.

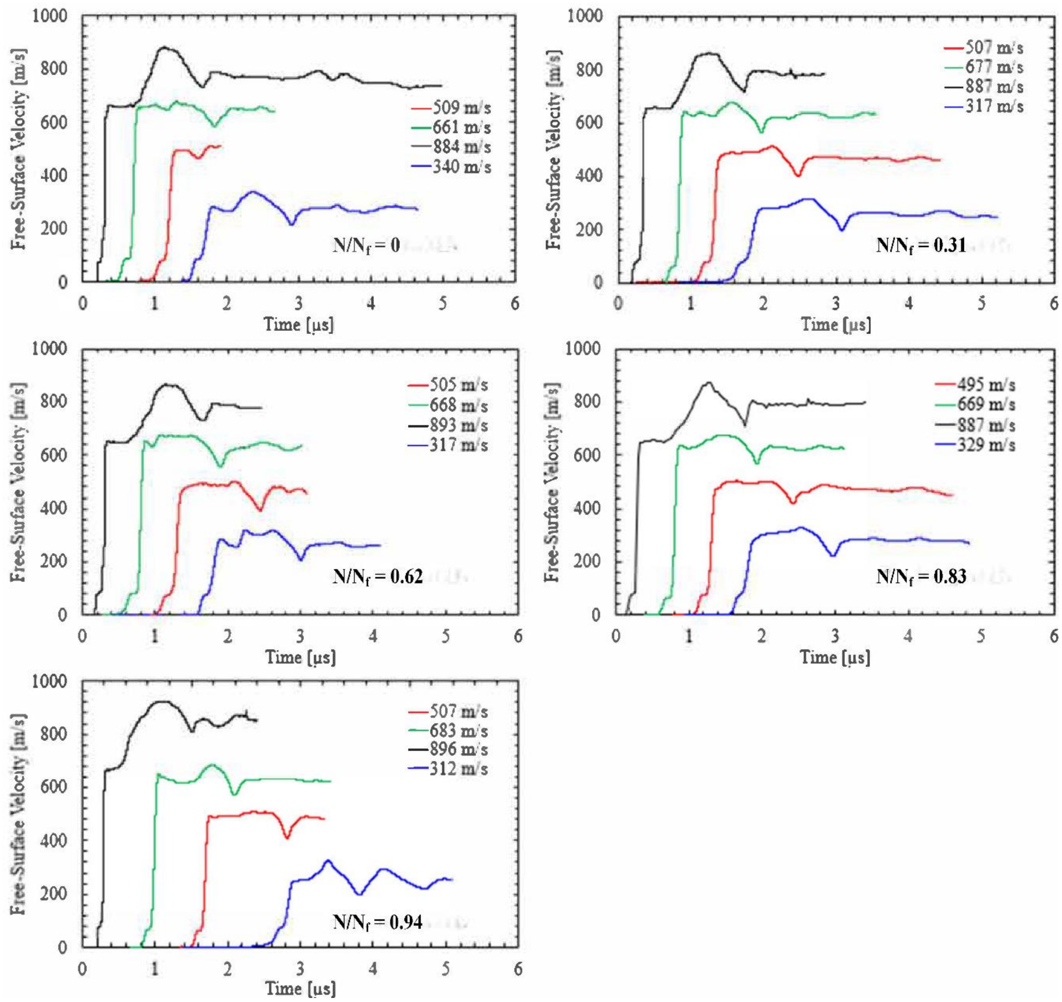

Figure 3. Velocity–time profiles extracted from velocimetry measurements at the free surface of the specimen. Velocities in each legend represent the respective velocities of the impactors just prior to impact.

No significant variation of the HEL is observed with increasing fatigue damage (Figure 4). Some reduction of the HEL is possible; however, error from the uncertainty relating to frequency variability in the measurements combined with the standard deviations of all four experiments per fatigue condition results in an error exceeding any possible loss of HEL strength. Typical fatigue damage exhibits a relatively low number of dislocations and will likely have minimal influence on a high-purity material in contrast to a work-hardened material, so the lack of drastic HEL softening may not be indicative of the response of other work-hardened BCC materials.[10,11]

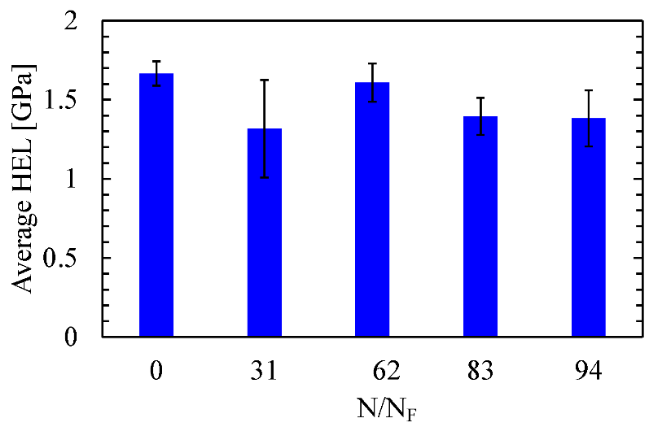

Figure 4. HEL averaged over four experiments per fatigue condition as a function of the number of cycles applied prior to shock load. Error bars represent the sum of the two most significant error sources, the standard deviation of four experiments and the error associated with frequency uncertainty.

A comparison of the bulk phase transformation stress as a function of fatigue damage in Figure 5 reveals a slight change in the transition stress from the α phase to the ε phase. From the pristine specimen to the one with the greatest fatigue damage, the phase transformation drops by less than 2%. Though a small percentage, it is significant given the relative stability of the phase transformation stress in pristine α-Fe.[6] Furthermore, the lowest phase transformation stress is the sample deformed to 0.83 N/N_f that exhibits a phase transformation stress approximately 6% below the pristine specimen. More in-depth microstructure analysis is required to comment on the mechanisms resulting in the reduced phase transformation stress. Undoubtedly, fatigue-induced damage generates porosity and a density of dislocations that has likely increased. These factors may contribute to increased local stress concentrations, localized severe plasticity, and reduced barrier stresses for nucleation and propagation of damage. In turn, these lead to a change in the applied stress required to initiate the phase transformation. However, such a discussion is limited to mere conjecture without a deeper characterization of the microstructure.

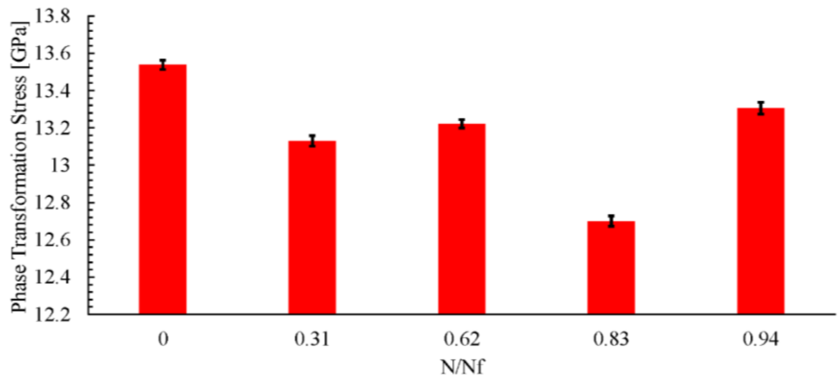

Figure 5. **Variability of the phase transformation measured in the bulk material with increasing fatigue damage. A sudden, though slight, drop in phase transformation stress is observed from the pristine to the fatigue-damaged material.**

The spall results of Figure 6a indicate that fatigue does have an influence on the spall strength of α-Fe. However, the mechanisms driving the differing behaviors are unclear. First, at low peak shock stress, the spall strength decreases with increasing fatigue damage, except for the highest fatigue damage case. Given the introduction of fatigue-generated damage, a reduction in spall strength may be expected. However, the trend of decreasing spall strength with increasing fatigue load does not hold for higher peak shock stresses. For the highest peak shock stress, spall strength appears to show the opposite response with an increasing spall strength coinciding with increased fatigue damage.

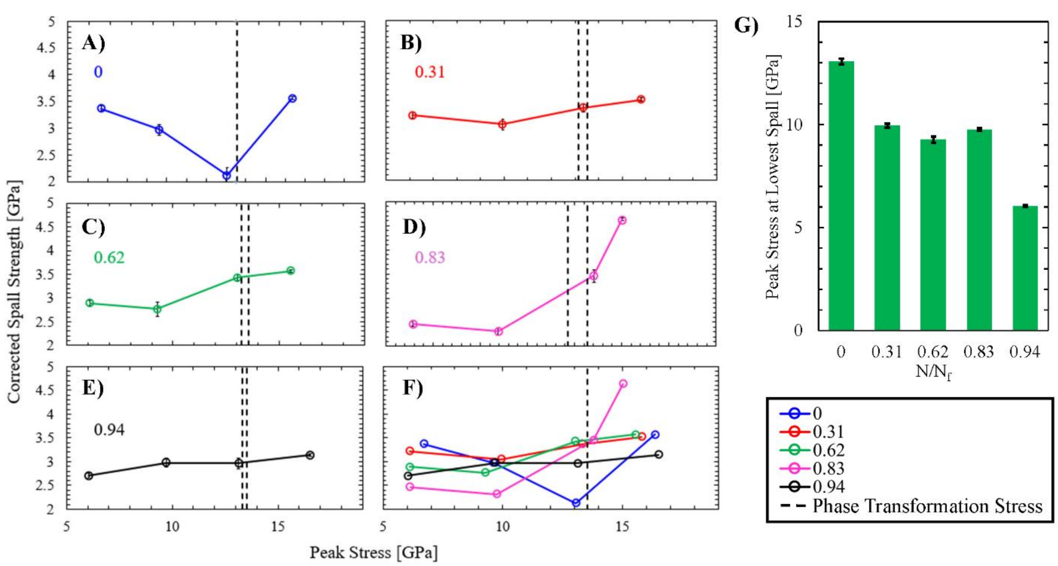

Figure 6. **(A–E) spall strength as a function of peak shock stress for each fatigue-loading condition. Dashed lines represent the phase transformation stresses of the undamaged material and the material damaged to the given fatigue condition, respectively. (F) compilation of the spall results for each fatigue-loading condition. (G) peak shock stress at which the minimum spall strength was measured for each fatigue-loading condition.**

As the peak shock stress approaches the phase transformation stress in α-Fe, the spall strength decreases. Once the phase transformation stress is exceeded, the material in the ε phase exhibits spall strengthening with increasing peak shock stress.[19,21] Looking at the cases with fatigue damage in Figures 6A through 6F in closer detail, the transition stress from spall softening to spall hardening appears to decrease below the phase transformation limit of undamaged α-Fe, as depicted more clearly in Figure 6G. The spall stress does not reach a minimum for the 0.94 N/N_f fatigued material except at the lowest peak shock stress analyzed in this work. Indeed, the results of the 0.94 N/N_f case show only a steady increase in spall strength. It is unclear how much of a role the reduced thickness of the specimens plays in this case, thus limiting any strong conclusions at the highest fatigue damage reported. Experiments where peak shock stress exceeds 13 GPa indicate the material's phase transformation stress is marginally reduced, but the spall data appears to indicate a more significant influence of this reduction in the phase transformation stress. According to Indeck et al.,[9] fatigue damage generates porosity with the largest measured volumes on the order of a few thousands of cubic microns. In 99.8% pure Fe, these are large enough to become a likely point for spall damage nucleation. Localized fatigue damage might result in severe plastic deformation and local heating upon the passing of the compressive shock wave, which results in an accelerated local phase transformation. If these points of severe plastic damage do not fully close the voids generated by fatigue loading, it is likely these same damaged regions would serve as the primary source for spall damage initiation. Further damage must then propagate through the severely deformed region where phase transformation preferentially occurs despite the bulk-mixed α-ε phase. To truly understand the cause of the drop in the critical peak shock stress at which the transition in spall behavior occurs, damage mechanisms must be investigated in greater depth through transmission electron microscopy studies coupled with shock and spall recovery experiments.

The undamaged material also exhibits voids of the same size and distribution as the 0.31 N/N_f and 0.62 N/N_f fatigue-damaged materials,[9] making it difficult to determine if the observations here are related to fatigue-generated porosity or other as yet undiscovered fatigue-generated microstructural changes. However, the reduction of the phase transformation stress and the peak stress for the transition from decreasing to increasing spall strength is apparent for both the 0.31 N/N_f and 0.62 N/N_f fatigued materials, so it is clear that fatigue damage does have an influence on the mechanical response to shock load. Due to the nature of cyclic loading where generation of fatigue-cycled materials is time- and resource-consuming, the damage characterization of these materials is limited. It is feasible that larger samples used for shock studies included large voids nucleated at lower levels of fatigue damage that were not captured by the initial damage analysis by

Indeck et al. Furthermore, few plate impact experiments can be completed within reasonable time due to the difficulties of producing fatigue-damaged materials. Minimum spall strength at similar peak shock stress was exhibited by the 0.31 N/N_f, 0.62 N/N_f, and 0.83 N/N_f specimens. This either indicates 1) the drop in phase transformation stress resulting from fatigue damage remains stable despite the degree of fatigue deformation generated or 2) the true critical peak stress at the transition from decreasing to increasing spall strength falls somewhere between 6 and 13 GPa, yet is only probed at roughly 9 GPa within this region. For the 0.94 N/N_f, the critical value falls somewhere below 9 GPa, but the only measurement performed below 9 GPa was a single measurement at roughly 6 GPa. The lack of a transition stress in the spall strength data may be an artifact of the smaller thickness of the 0.94 N/N_f specimens. It could also be an indicator that the critical stress at which the transition in the spall strength data occurs drops to a lower peak stress level despite a bulk phase transformation stress comparable with specimens of lower fatigue damage. Clearly, a greater body of work beyond the scope of this report is required to address these remaining questions.

4. Conclusion

The response of fatigue loaded α-Fe to dynamic uniaxial compressive strain and spall load was analyzed for α-Fe fatigued to varying percentages of the anticipated number of cycles to material failure. Fatigue damage was shown to cause no noticeable change in the HEL. However, the bulk phase transformation stress and the critical peak shock stress at which spall strength reaches a minimum value were shown to decrease with increasing fatigue damage. The phase transformation stress showed a sudden decrease of 2%–3% when fatigue damage was introduced and a 6% decrease that only applied to the case of 0.83 N/N_f. The critical transition stresses in the limited spall strength results did not perfectly correspond to the respective phase transformation stresses but did show a qualitatively similar decrease in value. These findings indicate that fatigue damage does influence the dynamic response of α-Fe, though the precise mechanisms governing the phase transformation stress and spall failure have not yet been determined. Further work should focus on deeper investigation into the initial microstructure and the post-shock and spall-recovered structures.

5. References

1. Lopez JG, Verleysen P, Degrieck J. Effect of fatigue damage on static and dynamic tensile behavior of electro-discharge machined Ti-6Al-4V. Fatigue Fract Eng Mater Struct. 2012;35:1120–1132.

2. Kawata K, Itabashi M, Kusaka S. Behaviour analysis of pre-fatigue damaged aluminum alloys under high-velocity and quasi-static tension. In: Pineau A, Zaoui A, editors. IUTAM Symposium on Micromechanics of Plasticity and Damage of Multiphase Materials. Springer; 1996. p. 394–404. https://doi.org/10.1007/978-94-009-1756-9_49

3. Paul SK, Sivaprasad S, Dhar S, Tarafder S. Cyclic plastic deformation and damage in 304LN stainless steel. Mater Sci Eng A. 2011;528:4873–4882.

4. Sanchez-Santana U, Rubio-Gonzalez C, Mesmacque G, Amrouche A. Effect of fatigue damage on the dynamic tensile behavior of 6061-T6 aluminum alloy and AISI 4140T steel. Int J Fatigue. 2009;31:1928–1937.

5. Duyi Y, Zhenlin W. Change characteristics of static mechanical property parameters and dislocation structures of 45# medium carbon structural steel during fatigue failure process. Mater Sci Eng A. 2001;297:54–61.

6. Barker LM, Hollenbach RE. Shock wave study of the $\alpha \rightleftarrows \varepsilon$ phase transition in iron. J Appl Phys. 1974;45:4872–4887.

7. Thomas SA et al. Dynamic strength properties and alpha-phase shock Hugoniot of iron and steel. J Appl Phys. 2018;123:175902.

8. Schijve J. Fatigue of structures and materials. Springer; 2009.

9. Indeck J, Cuadra J, Williams C, Hazeli K. Accumulation and evolution of elastically induced defects under cyclic loading: quantification and subsequent properties. Int J Fatigue. 2019;127:522–236.

10. Zaretsky EB, Kanel GI. Yield stress, polymorphic phase transformation, and spall fracture of shock-loaded iron in various structural states and at various temperatures. J Appl Phys. 2015;117:195901.

11. Millet JCF, Whiteman G, Park NT, Case S, Bourne NK. The role of cold work on the shock response of tantalum. J Appl Phys. 2013;113:233502.

12. Loree TR, Fowler CM, Zukas EG, Minshall FS. Dynamic polymorphism of some binary iron alloys. J Appl Phys. 1966;37:1918–1927.

13. Smith RF et al. Time-dependence of the alpha to epsilon phase transformation in iron. J Appl Phys. 2013;114:223507.

14. Farbaniec L, Williams CL, Kecskes L, Ramesh KT, Becker R. Microstructural effects on the spall properties of ECAE-processed AZ31B magnesium alloy. Int J Impact Eng. 2016;98:34–41.

15. Minich RW, Cazamias JU, Kumar M, Schwartz AJ. Effect of microstructural length scales on spall behavior of copper. Metallurg Mater Trans A. 2004;35A:2663–2673.

16. Galitskiy S, Mishra A, Dongare AM. Modeling shock-induced void collapse in single-crystal Ta systems at the mesoscales. Int J Plast. 2023;164:103596.

17. Lloyd JT, Ligda J, Williams CL. Pre-twinning alters shock-induced microstructure evolution in magnesium. Materialia. 2020;9:100606.

18. ASTM E466-15. Conducting force controlled constant amplitude axial fatigue testing of metallic materials. ASTM International; 2015.

19. Meyers MA. Dynamic behavior of materials. John Wiley & Sons, Inc.; 1994.

20. Zhang NB et al. Effects of shock-induced phase transition on spallation of a mild carbon steel. Int J Mech Sci. 2022;213:106858.

21. Zurek AK, Frantz CE, Gray GT 3rd. The influence of shock pre-strain and peak pressure on spall behavior of 4340 steel. International Conference on Shock-Wave and High-Strain-Rate Phenomena in Materials; 1990 Aug 12–17; San Diego, CA.

List of Symbols, Abbreviations, and Acronyms

1D	one-dimensional
α	alpha
AISI	American Iron and Steel Institute
ARL	Army Research Laboratory
BCC	body-centered cubic
c_l	static longitudinal elastic wave speed
DEVCOM	U.S. Army Combat Capabilities Development Command
Fe	iron
h	specimen thickness
HEL	Hugoniot elastic limit
h_i	impactor thickness
h_t	target thickness
N	number of load cycles
N_f	number of load cycles to failure
PDV	photon Doppler velocimetry
σ	resulting peak shock stress
t_e	elastic wave breakout time
t_s	shock wave breakout time
U_s	shock velocity
VISAR	velocity interferometer system for any reflector
v_0	impact velocity

1 (PDF)	DEFENSE TECHNICAL INFORMATION CTR DTIC OCA
1 (PDF)	DEVCOM ARL FCDD RLB CI TECH LIB